International Journal of Optomechatronics

ISSN: 1559-9612 (Print) 1559-9620 (Online) Journal homepage: https://www.tandfonline.com/loi/uopt20

Linear encoder based low frequency inertial sensor

Sylvain Hellegouarch, Lionel Fueyo Roza, Kurt Artoos, Pierre Lambert & Christophe Collette

To cite this article: Sylvain Hellegouarch, Lionel Fueyo Roza, Kurt Artoos, Pierre Lambert & Christophe Collette (2016) Linear encoder based low frequency inertial sensor, International Journal of Optomechatronics, 10:3-4, 120-129, DOI: 10.1080/15599612.2016.1217109

To link to this article: https://doi.org/10.1080/15599612.2016.1217109

Published online: 08 Sep 2016.

INTERNATIONAL JOURNAL OF OPTOMECHATRONICS
2016, VOL. 10, NOS. 3-4, 120–129
http://dx.doi.org/10.1080/15599612.2016.1217109

Taylor & Francis
Taylor & Francis Group

Linear encoder based low frequency inertial sensor

Sylvain Hellegouarch[a], Lionel Fueyo Roza[a], Kurt Artoos[b], Pierre Lambert[a], and Christophe Collette[a]

[a]BEAMS Department CP 165/56, Université Libre de Bruxelles, Brussels, Belgium; [b]Engineering Department, CERN, Geneva, Switzerland

ABSTRACT

In this article, we present a novel concept of inertial sensor, based on a linear encoder. Compared to other interferometric sensors, the encoder is much more easy to mount, and the calibration more stable. A prototype has been built and validated experimentally by comparison with a commercial seismometer. It has a resolution of about 10 pm/√Hz. In order to further improve the resolution, two concepts of mechanical amplifiers have been studied and compared. One of them is shown to be extremely promising, provided that the amplifier does not stiffen the sensor.

KEYWORDS

Inertial sensor; linear encoder; mechanical amplifier

1. Introduction

There exist a large variety of inertial sensors for seismic measurements in the low frequency range, say from 0.1 Hz to 50 Hz: seismic accelerometers, geophones and broadband seismometers. A comparison of these inertial sensors can be found in[1,2]. For thirty years, first choice instruments have had a resolution that is better than the lowest motion on Earth[3–6]. However, these instruments still suffer from a certain number of drawbacks, including being large, expensive, heavy, fragile, and sensitive to harsh environments. In order to bypass these limitations, several prototypes have been developed on the basis of an optical technology. For example, optical seismometers without electronics and insensitive to temperature and high pressure have been developed for the oil/gas and mining industry[7–9], which are capable of operating in harsh environments (e.g., down-holes, boreholes). Also, miniature accelerometers have been tested for the detection of nuclear tests conducted by countries engaged in nuclear proliferation[10].

Another emblematic example of application requiring efficient inertial sensor is active vibration isolation[11]. In an actively controlled platform, the vibrations are measured with inertial sensors, and are further cancelled using several actuators placed below the platform. Such platforms are increasingly used e.g., in lithography machines, atomic force microscopy, or large instruments dedicated to extreme experimental physics (gravitational wave detectors or future particle colliders). Various optical technologies have been already used in inertial sensors: fiber interferometer[12–14], Fabry-Perot interferometer[15], triangulation system[16], fiber Bragg grating[17–18], optical encoder[19], or grating sensor[20]. More recently, optical accelerometers based on Michelson interferometer have been proposed for measuring vibrations in gravitational wave detectors[21–23]. Figure 1 shows another prototype of optical sensor recently developed at the Université Libre de Bruxelles (ULB)[24]. It consists of a horizontal pendulum, connected to a rigid frame through a flexural joint, made of CuBe alloy. A leaf spring, made of the same alloy, is used to adjust the equilibrium position

CONTACT Christophe Collette ccollett@ulb.ac.be BEAMS Department CP 165/56, Université Libre de Bruxelles, 50, av. F.D Roosevelt, 1050 Brussels, Belgium.
Color versions of one or more of the figures in this article can be found online at www.tandfonline.com/uopt.

Nomenclature

M	= inertial mass of the sensor	H_1	= amplification factor of the first concept (Figure 8)
f_0	= first resonance frequency of the sensor	Θ	= tilt angle of the inertial rod in Figure 10
T	= restoring torque due to the stiffness of elastic hinge.	θ	= tilt angle of the secondary pendulum on which the scale is mounted.
K	= stiffness of the elastic hinge	y	= relative displacement between the scale and the sensor head.
α	= tilt angle of the inertial rod in Figure 8	L	= length of the rod on which the inertial mass is mounted in Figure 10
u	= ground displacement	l_3	= length from the rotation centre of the main pendulum to the connection with the secondary pendulum
l_1	= length of the rod on which the inertial mass is mounted in Figure 8. It is also the distance from the rotation center of the secondary pendulum and the connection with the main pendulum in Figure 10.	D	= length ratio L/l_3
l_2	= length of the rod on which the scale of the encoder is mounted (mechanical amplifier)	D	= length ratio l_2/l_1
xm	= motion of the inertial mass	γ	= ratio D/d
μ	= M/m = mass ratio	H_2	= amplification factor of the second concept (Figure 10).
β	= l_1/l_2 = length ratio		

of the inertial mass and compensate for gravity. The oscillator is characterized by an inertial mass $M = 0.055$ kg, a principal resonance frequency $f_0 = 6$ Hz and spurious resonances above 100 Hz. The relative displacement between the inertial mass and the support is measured with a Michelson interferometer, adapted to enable the measurement of both quadratures of the signals as in[7]. It has a resolution of 3 pm/√Hz above 4 Hz[24], which fits with the requirements for active stabilization of future linear particle colliders. However, besides this performance, a possible weakness of this sensor is that the calibration of the interferometer fluctuates over time, due to misalignment of the optical components. In this article, we will investigate the possibility to replace the Michelson interferometer by a linear encoder. The motivation for using a linear encoder is to avoid calibration issues,

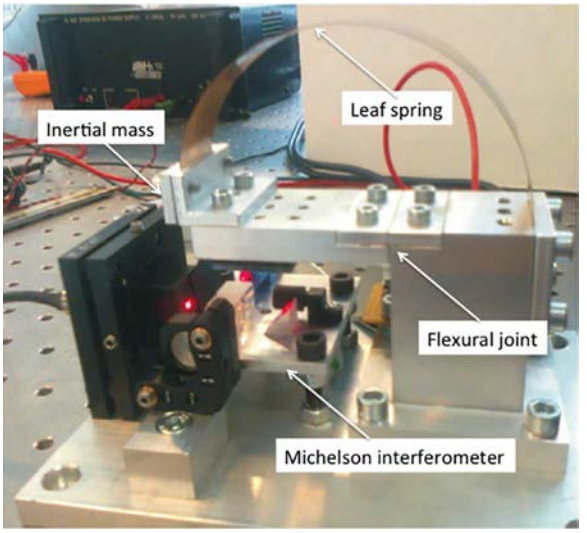

Figure 1. Picture of an interferometric inertial sensor[24]. It consists of a pendulum, connected to a rigid frame through a flexural joint. A leaf spring is used to adjust the static deflection of the inertial mass. The relative motion between the inertial mass and the rigid frame is measured by a homemade Michelson interferometer. The flexible joint is a leaf spring in CuBe material, with a thickness of 90 microns and a width of 5 cm.

without compromising the resolution. The objective of the work is to develop a robust inertial sensor with a resolution around 1-3 pm/√Hz above 4 Hz. To this aim, a first prototype of linear encoder based inertial sensor will be presented and validated. However, as its resolution is sill limited around 10 pm/√Hz, a strategy to further improve the resolution with a mechanical amplifier will be also presented in this article.

The article is organized as follows: Section 2 presents the performance of a linear encoder, selected as a good candidate for being integrated in an inertial sensor. Section 3 shows an experimental validation of the linear encoder based inertial sensor, section 4 presents two prototypes of mechanical amplifiers, and section 5 draws the conclusions and directions for improvements.

2. Linear encoder test bench

The linear encoder considered is a LIP281 from Heidenhain. In order to check the calibration, it has been mounted on a test bench shown in Figure 2, along with a Keyence LC-2440 and a geophone GS-11D. Both the LIP 281 and the LC-2440 measure the motion of the inertial mass of the mechanism. The linear encoder has been mounted on the synchronization lever and not on the compensated linear guide for space purpose. However, the angular error induced by the rotation of the lever is negligible. The mechanism has no spurious resonance below at least 500 Hz. The LIP 281 signals have been amplified by an operational amplifier INA118 to avoid ADC noise of the 16 bits recorder dSpace DS1103. Signals have been recorded with a sampling frequency of 10 kHz.

Figure 3 shows the Amplitude Spectral Densities (ASD) of the signals measured by the three sensors. In the frequency range around the resonance of the mechanism (around 7 Hz) the ASD of the LC-2440 and of the LIP 281 are superimposed. Above 10 Hz, the LIP 281 and the GS11D sense the same motion while the LC-2440 is dominated by ADC noise.

The resolution curves shown in Figure 4 have been obtained when the mechanism is blocked. Two amplifications are visible. The first one is between 5 Hz and 100 Hz; the second one is between 300 Hz and 600 Hz. The first one is presumably inherent to the sensor itself. The second can be due to resonances in the mount of the sensor head. Besides these resonances, the value of the ASD is around 10^{-11} m/√Hz, and decreasing around 10^{-12} m/√Hz at high frequency. The integrated RMS value (Figure 5) shows a resolution of 0.3 nm. The next section presents the prototype of inertial sensor using the optical encoder.

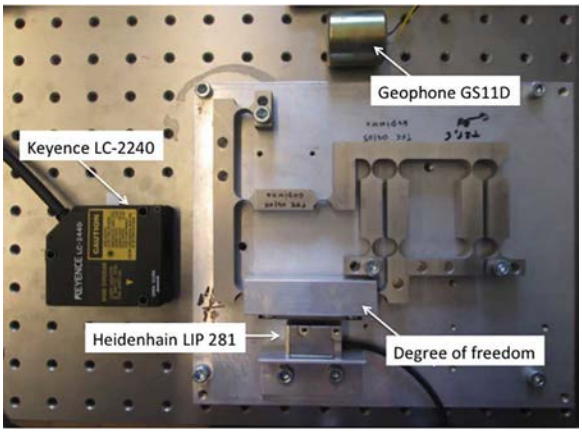

Figure 2. Picture of the experimental set-up used to calibrate the sensors. Both the LIP 281 and the LC-2440 measure the motion of the degree-of-freedom of the mechanism (no external actuation has been used). The mechanism is a double parallelogram, connected to an external arm for removing the internal degree-of-freedom. A geophone GS11D is also mounted besides the mechanism, oriented in the direction of the degree-of-freedom of the mechanism.

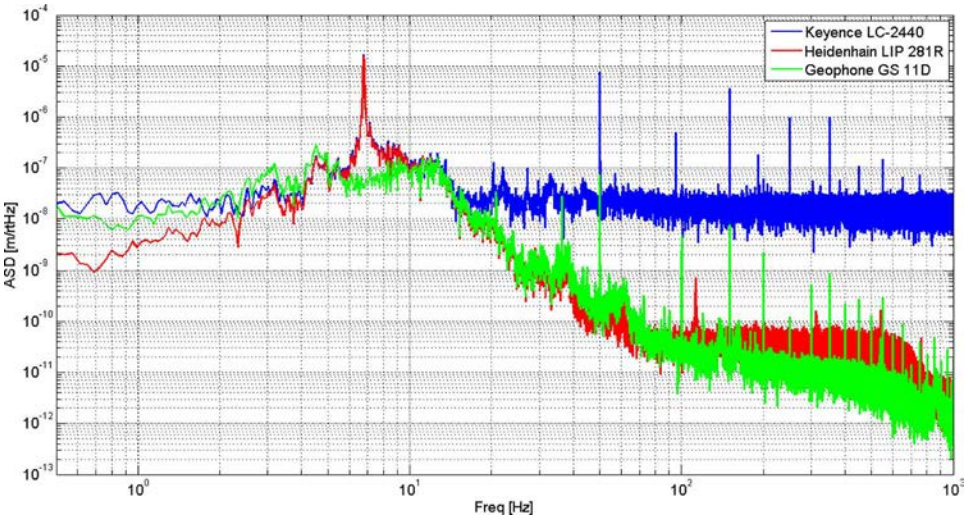

Figure 3. Amplitude Spectral Density (ASD) of the signals measured by the three sensors mounted on the mechanism shown in Figure 2. Signal calibration while the mechanism is moving freely in response to the ambient excitation: LIP and LC are identical above the noise. Geophone is also identical between 10 Hz and 20 Hz.

3. Prototype testing

Figure 6 shows a picture of the linear encoder based inertial sensor. In order to obtain its sensitivity curve, it has been mounted beside a commercial Guralp GMG-6T seismometer. The signal of both sensors have been recorded simultaneously using a DSpace DS1103.

Figure 7(*a*) and (*b*) respectively show the amplitude and phase of the transfer function between both sensors. As the sensitivity of the CMG-6 T is mainly flat in the frequency range shown, the signal from the seismometer has been simply integrated, and scaled by the sensitivity. The slight increase of the phase above 20 Hz is due to the phase drop in the GMG-6T sensitivity. Figure 7(*c*) is the coherence between the sensors, showing that the linear encoder based inertial sensor behaves as an inertial sensor. The curves have been obtained with a measurement of 105 s, with a sampling frequency of 10 kHz. These curves show that the prototype of linear encoder based inertial sensor behaves as an

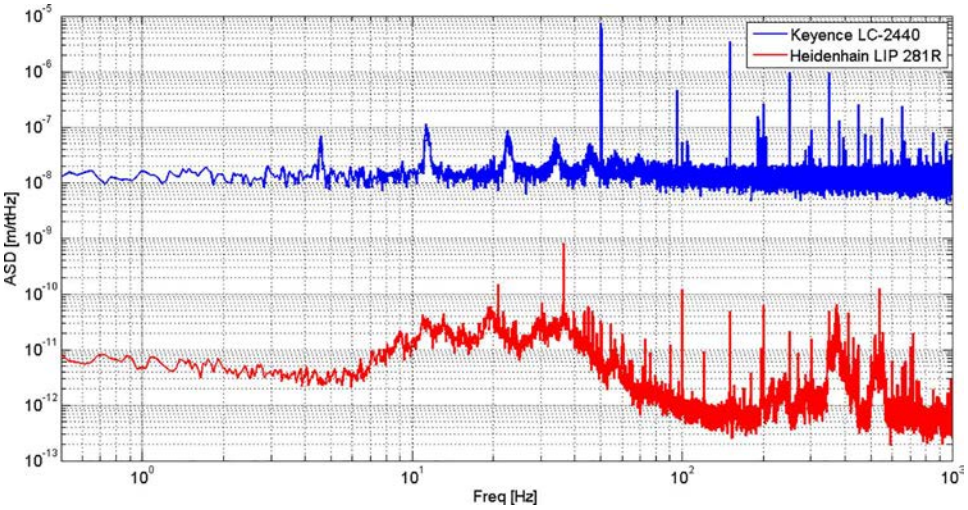

Figure 4. Resolution: ASD of the signals measured by the LIP and the LC when the mechanism is blocked.

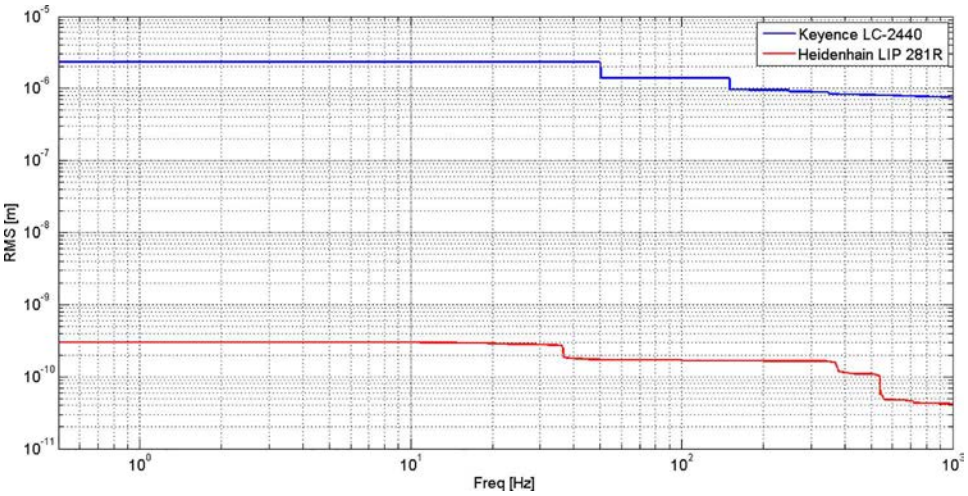

Figure 5. Integrated (downwards) RMS value of the resolution shown in Figure 4.

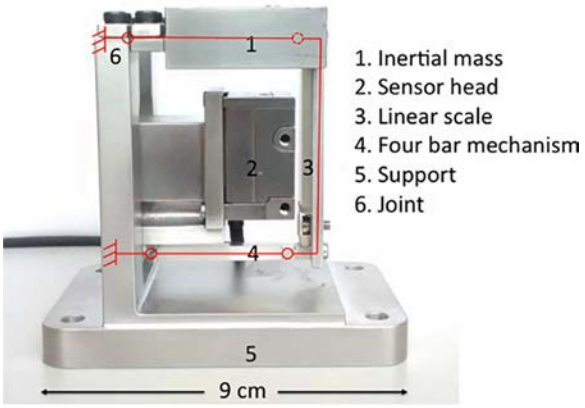

Figure 6. Picture of the linear encoder based inertial sensor.

absolute displacement sensor above 15 Hz, and as an accelerometer below 10 Hz. The coherence drop below 4 Hz is due to the finite length of the measurement.

In order to fulfill the requirement of future active isolation systems[30] an improvement of this value by a factor 2 to 5 is desirable. To this aim, it is proposed to use a mechanical amplifier, in order to magnify the relative motion between the inertial mass of the sensor and the support. Two concepts of mechanical amplification structures are studied and compared in the following section.

4. Inertial mechanical amplifiers

4.1. First concept

The first concept shown in Figure 8 consists of a rod balanced by two masses. M plays the role of the inertial mass and m represents the mass of the linear scale (i.e., the moving part of the linear encoder). The rod is connected to the ground trough an elastic hinge developing a restoring torque $T = -\mathrm{K}\,\alpha$. Due to the ground vibration u, the rod is tilted with an angle α. Considering the dynamic equation of the rod, we can write $\ddot{\alpha}$ as a function of $\ddot{u}$ and write the amplification factor of the mechanism as $\alpha l_2/u$. Indeed, it can be assumed that, above the resonance frequency of the pendulum, the fixed point of

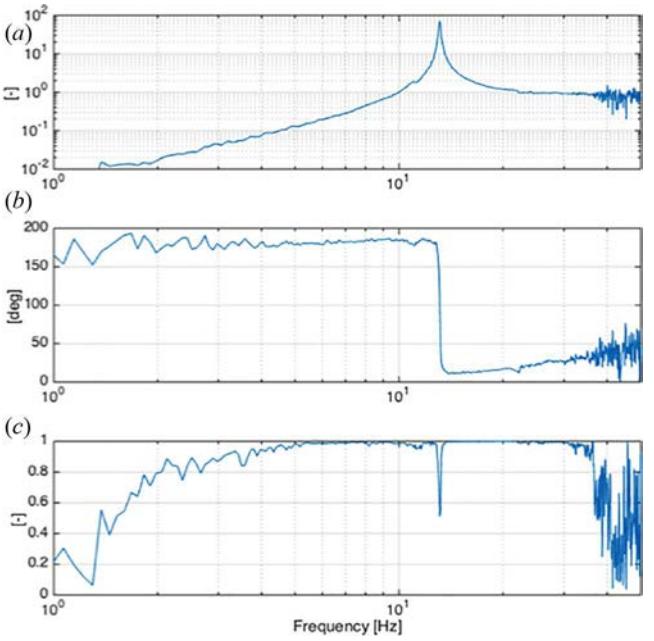

Figure 7. (*a*) Amplitude and (*b*) phase of the transfer function between a GMG-6T and the prototype of linear encoder based inertial sensor. (*c*) Coherence between the two signals.

the mechanism is located close to M, and the relative motion x_m-u measured by the encoder will correspond to the relative motion x-u amplified by the suspended bar.

After some manipulations, it can be shown that, above the resonance frequency of the oscillator, the amplification factor is:

$$H_1 = \frac{\alpha l_2}{u} = \frac{Ml_1l_2 - ml_2^2}{Ml_1^2 + ml_2^2}$$

or, upon defining $\mu = M/m$ and $\beta = l_1/l_2$,

$$H_1(\mu, \beta) = \frac{\mu\beta - 1}{\mu\beta^2 + 1}$$

The amplification $H_1(\mu, \beta)$ is shown in Figure 9 as a function of the mass ratio μ and of the length ratio β.

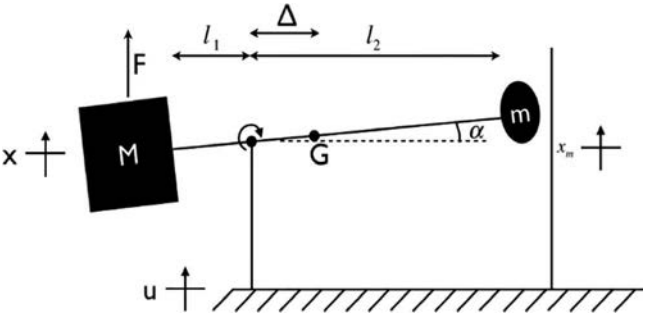

Figure 8. First concept of inertial mechanical amplifier. Above the resonance of the pendulum, as M ≫ m, a motion of the ground u will induce a larger motion of m. The encoder measure the relative motion (x_m-u) between m and the ground.

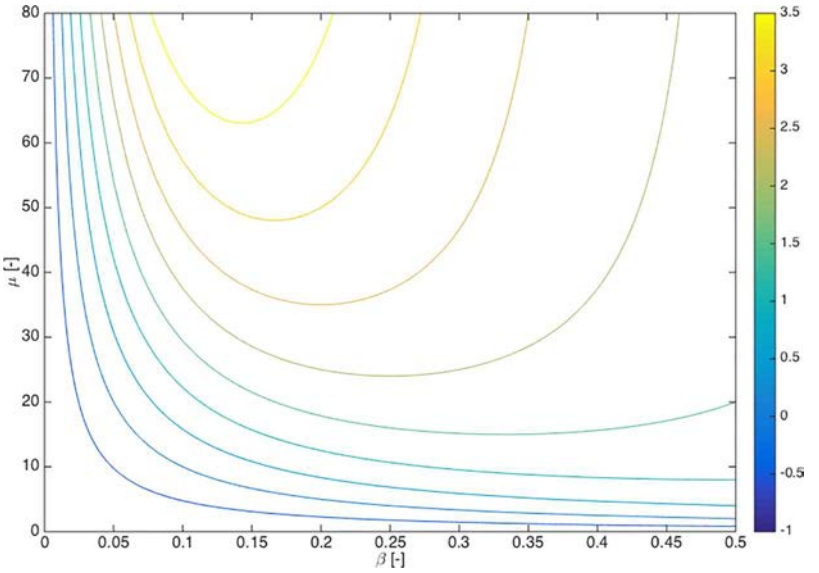

Figure 9. Mechanical amplification obtained using the first concept as a function of the mass ratio μ and of the length ratio β.

One sees in the figure that choosing $\beta = 0.15$ and $\mu = 70$ will lead to an amplification of more than a factor 3. However, a first weakness of the design is that, as m has a circular trajectory, the linear scale will be misaligned for large amplitudes. However, if the amplitude of vibration of the ground is large, the misalignment of the scale might distort the signal of the encoder. A second and more serious weakness is that it is difficult to combine a large amplification (i.e., increase of l_2) with a good rejection of spurious resonance modes, due to the lack of stiffness in the design (proportional to $1/l_2^3$). A second concept has consequently been developed, and presented in the next section.

4.2. Second concept

Figure 10 shows the working principle of the second amplification mechanism. It consists of a pendulum, on which is attached a mass M. Due to ground vibrations u, this pendulum tilts by an angle Θ. A second pendulum is cinematically coupled to the first one, through a rigid vertical link. The coupling ensures that $\Theta l_3 = \theta l_1$. Again, m represents the mass of the linear scale, used to measure the relative displacement $y = \theta l_2$.

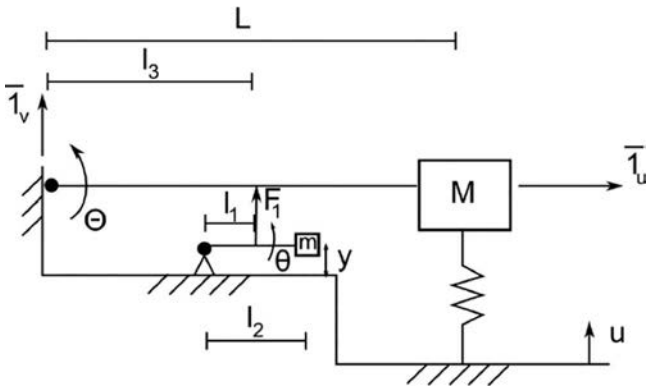

Figure 10. Second concept of inertial mechanical amplifier. Above the resonance of the mechanism, a motion of the ground will induce a larger motion of m. The encoder measures the relative motion (y) between m and the ground.

After some basic manipulation, the amplification factor $\theta l_1/u$ above the resonance frequency of the oscillator is found to be

$$H_2 = \frac{MLl_1l_2l_3 + ml_2^2l_3^2}{ML^2l_1^2 + ml_2^2l_3^2}$$

Defining $\mu = M/m$, $D = L/l_3$ and $d = l_2/l_1$ and $\gamma = D/d$, H_2 can be rewritten

$$H_2(\mu, \gamma) = \frac{\mu\gamma + 1}{\mu\gamma^2 + 1}$$

Note well that due to the topology difference in both mechanisms, l_1 and l_2 does not represent the same quantity in both mechanisms. Again, the amplification is shown in Figure 11 as a function of the mass ratio μ and of the length ratio γ. One sees in the figure that, compared to the first concept, a larger amplification can be reached, up to a factor 5 by choosing $\mu = 70$ and $\gamma = 0.1$.

Several prototypes have been developed on the basis of this second concept (see parameters in Table 1).

For each of them, a parallelogram has been used to reduce the inclination of the bar on which will be mounted the linear scale. The performances of four prototypes are compared in Figure 12 in a diagram reporting their mechanical amplification as a function of the fundamental eigen frequency of the system. The plot clearly shows that a large mechanical amplification is obtained at the cost of an increase of the resonance frequency, because of the internal stiffness of the amplification mechanism. Unfortunately, it will in turn decrease the sensitivity of the accelerometer in the frequency

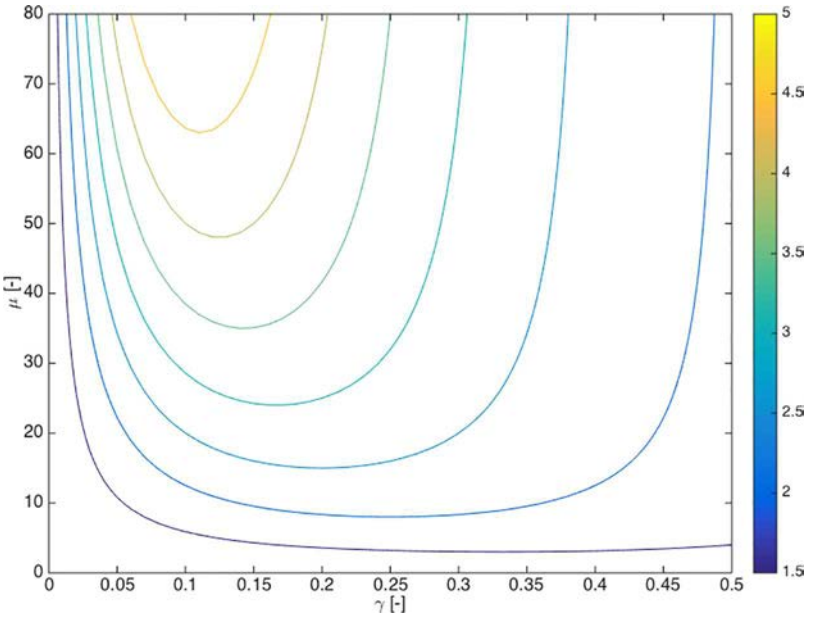

Figure 11. Mechanical amplification obtained for the second concept as a function of the mass ratio μ and the length ratio γ.

Table 1. Parameters chosen for each of the 4 designs based on the second concept and related amplification factor H_2.

	Design 1	Design 2	Design 3	Design 4
M (g)	472	472	225	222
H_2	2.07	3.7	5.3	12.3
First natural frequency (Hz)	10	17.5	36.8	77

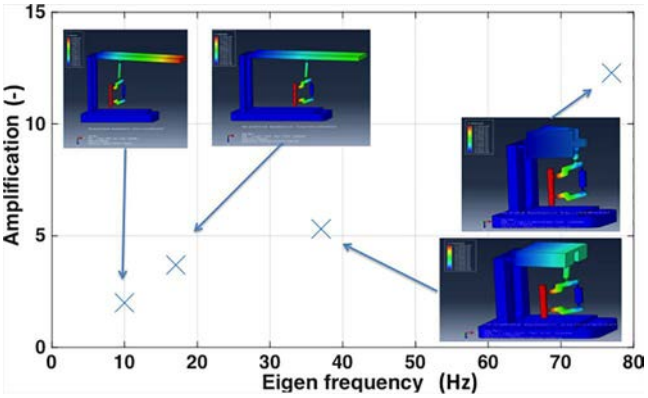

Figure 12. Tradeoff between the first resonance frequency (to decrease) and motion amplification (to increase) for several prototypes of mechanically amplified inertial sensors.

range below its resonance. One possible solution to this problem will be to add a negative stiffness in the design, in order to maintain the amplification, without any increase of the natural frequency. This study is left for a future work.

5. Conclusions

This article has presented a small prototype of linear encoder based inertial sensor. This prototype follows a previous one, which was based on a Michelson interferometer. In order to balance the lack of robustness of the interferometer, a linear encoder has been considered as an alternative sensor to measure the relative motion between the support and the inertial mass. Compared to the interferometer, the encoder is much less sensitive to misalignments. A first prototype of linear encoder based inertial sensor has been built and validated experimentally by placing it close to a commercial GMG-6T, and comparing the signals from the two sensors.

In order to further increase the resolution, two concepts of mechanical amplifier have been proposed and compared. Four designs based on the second concept have been developed, trying to maximize the ratio between the mechanical amplification over the resonance frequency of the mechanical system. The optimization process revealed that a trade-off exists between these quantities because the amplifier has its own stiffness/mass.

In a future work, the sensor will be upgraded with a low-stiffness low-mass mechanical amplifier.

Acknowledgments

The reviewers are also warmly acknowledged for their valuable comments, which have significantly contributed to improve the quality of the manuscript.

Funding

The authors gratefully acknowledge the Brussels Capital Region and the FNRS for funding and supporting this research.

References

[1] Wienlandt, E. Seismometry. In: International Handbook of Earthquake and Engineering Seismology, Part A; Lee, W.H.K.; Kanamori, H.; Jennings, P.C.; Kisslinger, C. Eds.; Academic Press: Amsterdam, 2002; pp. 283–304.

[2] Collette, C.; Janssens, S.; Fernandez-Carmona, P.; Artoos, K.; Guinchard, M.; Hauviller, C.; Preumont, A. Review: Inertial sensors for low-frequency seismic vibration measurement. *Bull. Seismol. Soc. Am.* **2012**, *102*, 1289–1300.

[3] Sheffield, H.E. An electronic vertical long-period seismometer. *IEEE Trans. Inst. Meas.* **1964**, *13*, 2–7.
[4] Teupser, C.; Plesinger, A. Design of feedback-controlled wide-band seismo-graphs with respect to undesired side-effects. *Phys. Earth Planet. Inter.* **1979**, *18*, 58–63.
[5] Usher, M.J.; Burch, R.F.; Guralp, C. Wide-band feedback seismometers. *Phys. Earth Planet. Inter.* **1979**, *18*, 38–50.
[6] Wielandt, E.; Sterkeisen, G. The leaf spring seismometer: Design and performance. *Bull. Seismol. Soc. Am.* **1982**, *72*, 2349–2367.
[7] Zumberge, M.; Berger, J.; Otero, J.; Wielandt, E. An optical seismometer without force feedback. *Bull. Seismol. Soc. Am.* **2010**, *100*, 598–605.
[8] Otero, J. Development and Characterization of an Observatory-class, Broad-band, Non-Fedback, Leaf-Spring Interferometric Seismometer (PhD thesis), University of California, San Dego, 2009.
[9] Zumberge, M.; Berger, J.; Wielandt, E. Optical seismometer, US patent2012/0247213 A1, 2012.
[10] Carr, D.; Baldwin, P.; Knapp-Kleinsorge, S.; Milburn, H.; Robinson, D. A laser interferometric miniature seismometer, In: *Monitoring Research Review: Ground-Based Nuclear Explosion Monitoring Technologies*, 2011, pp. 258–265.
[11] Collette, C.; Janssens, S.; Artoos, K. Review of active vibration isolation strategies. *Recent Patents Mech. Eng.* **2011**, *4*, 212–219.
[12] Gardner, D.; Hofler, T.; Baker, S.; Yarber, R.; Garrett, S. A fiber-optic interferometric seismometer. *J. Lightwave Technol.* **1987**, *5*, 953–960.
[13] Araya, A.; Kawabe, K.; Sato, T.; Mio, M.; Tsubono, K. Highly sensitive wideband seismometer using a laser interferometer. *Rev. Sci. Instrum.* **1993**, *64*, 1337–1341.
[14] Araya, A.; Sekiya, K.; Shindo, Y. Broadband seismometer for ocean bore-hole observations. In: *Symposium on Underwater Technology and Workshop on Scientific Use of Submarine Cables and Related Technologies*, Tokyo, 2007, 245–248.
[15] Littler, I.; Chow, J.; Mcclelland, D. A system, device and method for detecting seismic acceleration. **2010**, WO2010057247.
[16] Chatrefou, D. Optical vibration sensor. **1999**, US5886265.
[17] Levine, B. Simple fiber optic seismometer for harsh environments. **2007**, US7714271.
[18] Anderson, J. Fiber optic microseismic sensing systems. **2011**, WO201150275.
[19] Cahill, R.; Udd, E. Optical vibration sensor. **1984**, US4471659.
[20] Merchant, B.; Okandan, M. *The SNL MEMS seismometer: Design and testing.* In: *Monitoring Research Review: Ground-Based Nuclear Explosion Monitoring Technologies*, 2009, pp. 352–358.
[21] Acernese, F.; Giordano, G.; Romano, R.; De Rosa, R.; Barone, R. Mechanical monolithic horizontal sensor for low frequency seismic noise measurement. *Rev. Sci. Instrum.* **2008**, *79*, 074501.
[22] Acernese, F.; Giordano, G.; Romano, R.; De Rosa, R.; Barone, R. Tunable mechanical monolithic sensor with interferometric readout for low frequency seismic noise measurement. *Nucl. Instrum. Methods Phys. Res. A* **2010**, *617*, 457–458.
[23] Acernese, F.; Giordano, G.; Romano, R.; Barone, R. Compact tunable monolithic sensors for vibration monitoring and control of structures and very low frequency large band characterization of sites. In: *15th World Conference in Earthquake Engineering*, Lisbon, Portugal, September 24–28, 2012; Sociedade Portuguesa de Engenharia Sismica (SPES): Lisbon, Portugal; 2012.
[24] Collette, C.; Nassif, F.; Amar, J.; Depouhon, C.; Gorza, S.-P. Prototype of interferometric absolute motion sensor. *Sensors and Actuators A: Physical* **2015**, *224*, 72–77.